Available online at www.sciencedirect.com
SCIENCE DIRECT®
Journal of Power Sources 139 (2005) 35–43
JOURNAL OF POWER SOURCES
www.elsevier.com/locate/jpowsour

A modeling investigation on the electrochemical behavior of porous mixed conducting cathodes for solid oxide fuel cells

Yanwei Zeng*, Changan Tian, Limei Bao

School of Materials Science and Engineering, Nanjing University of Technology, Nanjing 210009, PR China

Received 17 March 2004; received in revised form 5 July 2004; accepted 14 July 2004
Available online 15 September 2004

Abstract

The electrochemical behaviors of porous mixed conducting cathodes for solid oxide fuel cells have been quantitatively investigated in this paper through numerical simulations on 1D and 2D porous models by using analytical approach and finite element method. A clear and comprehensive picture about the cathode overpotentials and current density distributions has been revealed as a convoluted function of cathode's oxygen surface reaction kinetic rate constant, ionic bulk conductivity, geometric size and pore structures. On the basis of simulation results, extended discussions were also made on the impacts of structural heterogeneities including the pores and the graded interfacial structure composed of a single phase and dual phases in the area bordering electrolytes on the effective cathode areal resistance that may be adopted to characterize the electrochemical behavior of cathodes.

Keywords: Overpotentials; Current density distribution; Porous mixed conducting cathode; Finite element method; Numerical modeling

1. Introduction

Solid oxide fuel cells (SOFCs) are widely known as one of the most potential environmentally benign power generators with superior energy-convert efficiency. However, their commercial realization is being faced with challenges from the requirements for the materials with high electrochemical performance and long-term thermal/chemical stabilities. The development of SOFCs that can operate at intermediate temperatures of 600–800 °C can technically relax strains on the materials high temperature chemical stabilities but tough demands remain on the materials electrochemical properties, especially on the cathode materials that are committed to effectively fulfill oxygen incorporation into the system of SOFCs [1–8].

There is a general consensus that the overall electrochemical performance of a SOFC is basically associated with the material properties of each cell's component and the cell's structures, yet of them the kinetics of oxygen incorporation into cathodes and the following ionic transports are of particular importance because they often account for most of cell's overpotential losses [9–12]. Amid many cathode materials, one of the most extensively studied is doped $LaMnO_3$ that is of perovskite-type structure and possesses high electronic but rather low ionic conductivities. It is usually blended with YSZ and prepared into porous forms to build up abundant air-electrode-electrolyte three-phase boundaries (TPBs), where oxygen species after surface diffusion from their adsorption sites are thought to receive electrons and then commence its transport within the imbedded YSZ phase. In this kind of cathode materials, oxygen adsorption onto the surface of cathode, molecular dissociation and diffusion along the cathode surface towards TPBs, complete ionization and then transport in the electrolyte phase constitutes an oxygen cathodic reaction chain [13–16]. The process that takes place in the narrow TPB zones is commonly regarded as the most probable rate-determining step. In contrast to the electronically conducting materials of sort of doped $LaMnO_3$, a category of cathode materials with mixed ionic and electronic

* Corresponding author. Tel.: +86 25 8358 7254; fax: +86 25 8358 8316.
E-mail address: zengyanwei@163.net (Y. Zeng).

0378-7753/$ – see front matter © 2004 Elsevier B.V. All rights reserved.
doi:10.1016/j.jpowsour.2004.07.017

conductivities has attracted much research interest in recent years. Their dual electric conductance enables the oxygen species simply to start up its bulk transport inside cathodes from the surface location where it is adsorbed and dissociated. This conductive characteristic actually makes unnecessary the cross-transfer of oxygen species from the cathode to its bordering electrolyte phase around narrow TPBs areas and, therefore, leads to an enormous enhancement in the electrochemical performance of SOFCs. It is for this property that the mixed ionic and electronic conductors (MIEC) are nowadays considered the most promising cathode materials for commercially viable intermediate temperature SOFCs [17–19]. Over the past years, diverse experimental research efforts have been devoted to this family of materials with aims to improve or upgrade materials properties, including ionic conductivity and chemical/thermal stability and compatibility with electrolytes [19–32]. Some informative theoretical and modeling studies have also been performed for better understanding those fundamental issues involved in MIEC cathodes [33–41]. So far, nevertheless, a clear and comprehensive understanding of the electrochemical behavior of porous MIEC cathodes, especially, its quantitative relations to the materials properties, geometric dimensions, pore structures and electrochemical working conditions have not been achieved yet.

In this paper a numerical simulation of the electrochemical behavior of porous MIEC cathodes is reported, which has been performed on both 1D and 2D models. In particular, the overpotentials, ionic current density distributions and effective areal resistances of porous MIEC cathodes were numerically simulated by analytical approach and finite element method as a complex function of cathode's bulk ionic conductivity, effective oxygen surface incorporation kinetic rate constant, pore structures and geometric sizes. A wide discussion based on the simulation results have also been carried out to explore and disclose how the electrochemical behavior of a porous MIEC cathode is controlled by its oxygen surface incorporation kinetics, bulk ionic conductance, geometric sizes as well as microstructures. It is expected to help further clarify and quantitatively differentiate the convoluted contributions from these factors to the overall electrochemical performance of a porous MIEC cathode and, therefore, to offer an instructive guide to the development of SOFCs with prospective properties.

2. Models and theoretical considerations

2.1. 1D model

As schematically shown in Fig. 1, the basic structure of a cathode-electrolyte half cell for simulation studies is assumed to be constructed of a dense electrolyte membrane (bottom layer), a porous mixed conducting cathode (intermediate layer), and a gas-permeable metallic coating atop the cathode for electric current collection, where oxygen is

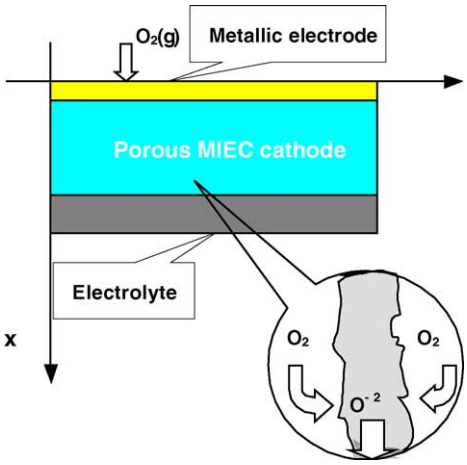

Fig. 1. Schematic diagram of cathode-electrolyte half-cell.

allowed to easily diffuse from outside into the pore channels of cathode and then to move onto its inner surfaces. Also, all the three layers are considered to be structurally uniform regardless of their microstructural details. When the half-cell's planar dimensions are much larger than its thickness as in a usual case, the infinite plate model is applicable to describing oxygen diffusion in the pores and ionic transport in the solid phase. Thus, a column with a cross-sectional area A, taken out of the half-cell in parallel to the direction of thickness, can be regarded as a representative of the half-cell for the description of its electrochemical behavior. Furthermore, when the structural homogeneity in the cathode and electrolyte is very high, the cross-sectional area A may be contracted into such a very small one that the representative column turns into a quasi 1D bar.

On the basis of such a 1D model, when a steady state of the cathode surface reaction at a given oxygen concentration is reached, the ionic current density at a depth x from the metal-cathode interface may be determined by

$$j = -\sigma_c \left(\frac{dv}{dx}\right) \tag{1}$$

and it must equal the total current density injected from the inner surface of cathode across the depth from *0* to *x*:

$$j = -\sigma_c \left(\frac{dv}{dx}\right) = \int_0^x \sigma_s(v_o - v)d\xi \tag{2}$$

where v refers to the potential at the depth x, induced by oxygen ion distribution in the cathode, v_o is the equilibrium potential determined by Nernst equation with respect to the given oxygen concentration, σ_c is the bulk ionic conductivity of cathode, and σ_s stands for an effective oxygen surface incorporation rate constant of cathode, which is actually a complex kinetic parameter proportional to the surface area per unit volume of cathode and closely associated with oxygen-related processes including gas diffusions within the pore

channels and towards the cathode surface, surface adsorption and ionization at a given system pressure and temperature.

By differentiating Eq. (2) with respect to x, a simple differential equation for 1D cathode potential distribution may be immediately reached:

$$\frac{d^2u}{dx^2} - \sigma u = 0 \tag{3}$$

where $\sigma = \sigma_s/\sigma_c$ and $u = v_o - v$. To perform analyses of cathode electrochemical behavior, a set of appropriate and particular boundary conditions is needed to match with above equation and in this paper the following conditions were employed:

$$\left(\frac{du}{dx}\right)_{x=0} = 0, \qquad \left(\frac{du}{dx}\right)_{x=t_c} = \frac{q}{\sigma_c} \tag{4}$$

It means that the ionic current density at $x = 0$ and $x = t_c$ (total thickness of the cathode) are respectively defined as null and q. Consequently, it follows from Eqs. (3) and (4) that:

$$v(x) = v_o - \frac{q[\exp(\sqrt{\sigma}x) + \exp(-\sqrt{\sigma}x)]}{\sigma_c\sqrt{\sigma}[\exp(\sqrt{\sigma}t_c) - \exp(-\sqrt{\sigma}t_c)]} \tag{5}$$

This equation gives a whole potential profile over the cathode thickness as a function of variable q and the relevant materials parameters and geometric thickness of the cathode. With the help of Eq. (2), it also gives the corresponding current density distribution.

2.2. 2D models

In order to fulfill a direct comparison with the results from above 1D model and to understand the impacts of microstrucural heterogeneity in a porous MIEC cathode on its electrochemical behavior, two 2D belt-like models have been constructed. One is called solid belt model with no microscopic pores in it and the other is a porous one containing a number of micro-sized pores. In the former model, the oxygen incorporation is assumed to take place along the two lateral sides of the belt while in the latter such a process is confined at the pore-cathode interfaces with the geometric details to be given in the following section. With these assumptions and in view of no current source inside cathode's solid phase, a 2D Poisson equation coupled with the boundary conditions below has been used for the potential description in above 2D models:

$$\nabla^2 v = \frac{\partial^2 v}{\partial x^2} + \frac{\partial^2 v}{\partial y^2} = 0 \tag{6}$$

$$-\sigma_c \vec{n}\nabla v = \sigma_s(v_o - v)_{\text{interfaces/laterals}}$$

where $\vec{n}$ is the unit vector normal to the relevant boundaries and the other parameters have the same meaning as in the case of 1D model. The conditions for the rest boundaries were so determined that no ionic current was allowed to pass except at the cathode-electrolyte interface where an average current density q was set:

$$-\vec{n}\nabla v = 0, \qquad -\sigma_c(\nabla v)_{c-e} = q \tag{7}$$

To reach the particular numerical solutions of Eq. (6), a finite element method based on Matlab computing language by The Mathworks, Inc. was utilized.

3. Results and discussions

3.1. Potential and current density distributions

As a prime result, the electric potential and ionic current density distributions across the thickness of cathode are shown in Fig. 2. They were calculated as a function of the current density q ranging from 0 to 5 (A cm^{-2}) when the equilibrium potential v_o was set as 1000 mV and the relevant model parameters were set: $\sigma_s = 5 \times 10^{-5}$ (S cm^{-1}), $\sigma_c = 1 \times 10^{-2}$ (S cm^{-1}), $t_c = 120\,\mu$m. It can be evidently noted that the cathode potential not only decreases in proportion to the magnitude of q but also shows an increasing descent as the depth x increases, accompanied by a parallel growth in the ionic current density along the cathode. These results are rather analogous to what was given by ALB model [36,37], characterized by a narrow electrochemically active region situated nearby the cathode-electrolyte interface from which most of the ionic current flowing into the electrolyte originates. It has been estimated that a region adjacent to the electrolyte providing 90% of the total ionic current is about 33 μm wide against a total cathode thickness of 120 μm.

Now let us move to the discussions on the porous cathode overpotentials, including surface overpotential and ionic transport overpotential stemming respectively from the chemical activation required for oxygen incorporation from the gaseous phase onto the cathode surface and the ensuing

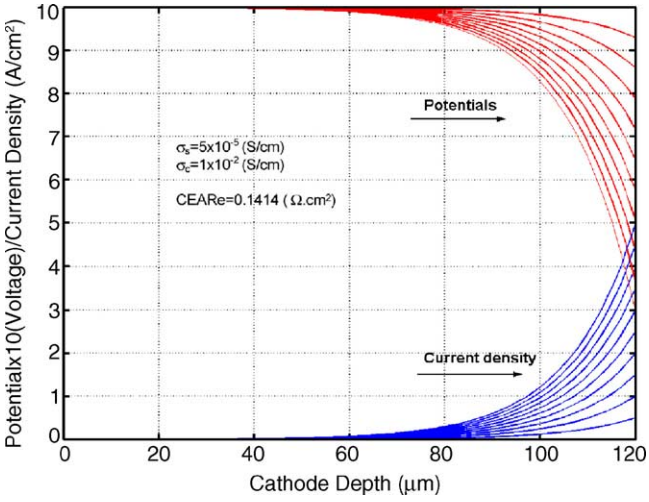

Fig. 2. Potential and current density distributions at different output current densities from 0 to 5 (A cm^{-2}).

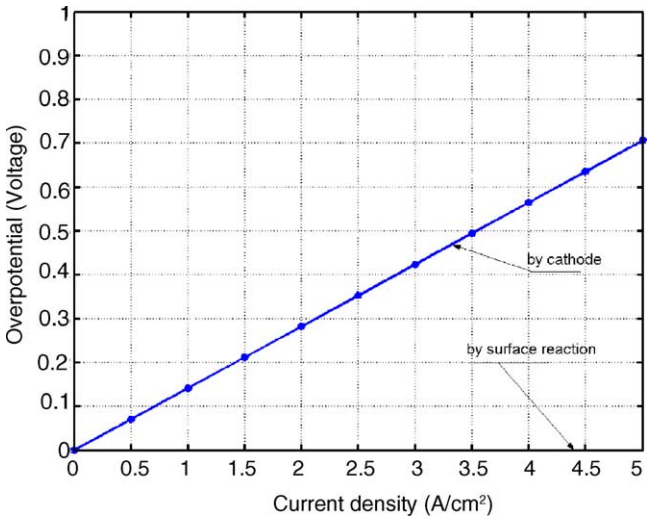

Fig. 3. Cathode overpotentials vs. current density.

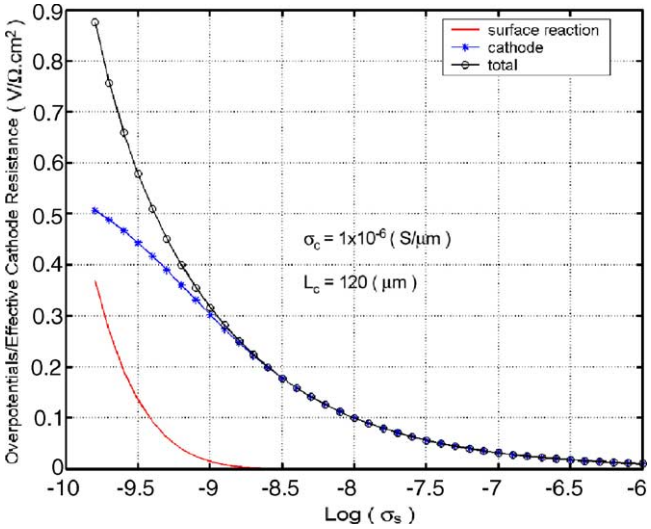

Fig. 4. Overpotentials or effective areal resistances vs. log (σ_s).

ionic bulk transport. From each of the above potential distributions, a potential drop at $x = 0$ and a total cathode overpotential can be easily obtained. The former may be directly regarded as the surface potential drop and, thus, the ionic transport overpotential equals the total cathode overpotential minus the surface potential drop. They both have been found to show a linear increase in proportion to the current density, as shown in Fig. 3. But the surface potential drop accounts only for 0.04% of the total and the latter does for 99.96% for the above given model parameters. These results explicitly indicate that the kinetics of electrochemical process in this case is overwhelmingly controlled by the ionic transport step. Nevertheless, it has been revealed by simulations that the effective oxygen surface reaction rate constant σ_s may remarkably affect the cathode overpotentials. Any changes in σ_s may make the electrochemically active region remarkably contract or expand so that the surface potential drop changes a lot and the reaction rate-determining step may switch from oxygen transport to oxygen surface incorporation or vice versa. The quantitative simulation results for this point have manifested, as illustrated in Fig. 4, that the surface potential drop grows unremarkably before $\log(\sigma_s) = -8.5$ as $\log(\sigma_s)$ decreases whereas, after that point, it may increase very fast up to a magnitude comparable to or even over the contribution from oxygen ionic transport.

3.2. Effective cathode areal resistances

It is well known that overpotential losses are practically caused by the resistance against ionic currents in the materials. For the pure ionic transport in an electrolyte, the overpotential is dependent on the flowing current density with a following proportional factor:

$$R_e = \frac{t_e}{\sigma_e} \tag{8}$$

where t_e is the thickness of electrolyte and σ_e its ionic conductivity. R_e is often called areal resistance of the electrolyte. The same notion is here applied to a porous MIEC cathode where complex electrochemical processes are involved due to inhomogeneous oxygen surface reactions and ionic transports. With the help of Eqs. (5) and (8), the effective areal resistances and the corresponding effective thickness for porous MIEC cathodes can be derived as follows:

$$R_{ct} \equiv \frac{v_o - v(t_c)}{q} = \frac{\exp(\sqrt{\sigma}t_c) + \exp(-\sqrt{\sigma}t_c)}{\sigma_c\sqrt{\sigma}[\exp(\sqrt{\sigma}t_c) - \exp(-\sqrt{\sigma}t_c)]} \tag{9}$$

$$R_{cs} = \frac{2}{\sigma_c\sqrt{\sigma}[\exp(\sqrt{\sigma}t_c) - \exp(-\sqrt{\sigma}t_c)]} \tag{10}$$

$$T_{ceff} \equiv R_{ct}\sigma_c = \frac{\exp(\sqrt{\sigma}t_c) + \exp(-\sqrt{\sigma}t_c)}{\sqrt{\sigma}[\exp(\sqrt{\sigma}t_c) - \exp(-\sqrt{\sigma}t_c)]} \tag{11}$$

where R_{cs} is called effective surface resistance corresponding to the surface potential drop. It can be seen that, unlike in the case of a simple electrolyte, the effective areal resistance of a porous MIEC cathode varies as a complex function of cathode thickness, oxygen ionic conductivity as well as a kinetics-related oxygen surface reaction rate constant σ_s, rather than a plain material parameter. The effective cathode thickness is now determined not only by the real geometric thickness of cathode and by a kinetics-related ratio of σ_s/σ_c as well.

To reach a quantitative understanding of the above points, several calculation graphic results are presented in Fig. 5, where three curved surfaces clearly depict the dependence of effective cathode areal resistance R_{ct}, effective oxygen surface reaction resistance R_{cs} and effective oxygen transport resistance R_{cb} on the cathode ionic conductivity σ_c and oxygen surface reaction rate constant σ_s when the real thickness is fixed at 120 μm. Fig. 6 gives a series of equal-resistance contours at $R = 0.1, 0.3, 0.5, \ldots, 5(\Omega\,\mathrm{cm}^{-2})$ with a constant interval of 0.2. It is clearly demonstrated that when the magnitude of $\log(\sigma_c)$ is relatively large, the effective cathode areal

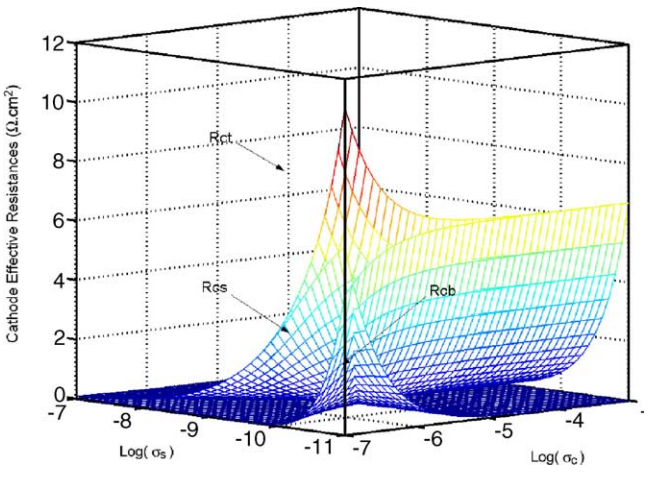

Fig. 5. Effective areal resistances versus oxygen surface reaction rate σ_s and ionic conductivity σ_c.

resistance R_{ct} increases rapidly and is mainly accounted for by oxygen ionic transport as the oxygen surface reaction rate decreases from around $\log(\sigma_s) = -7$. But, when the $\log(\sigma_c)$ becomes smaller, a decrease in $\log(\sigma_s)$ boosts a conspicuously increasing contribution R_{cs} from the cathode surface reaction to R_{ct} after certain critical value of $\log(\sigma_s)$ is overcrossed. In addition, as the ionic conductivity decreases, the resistance R_{cb} from ionic bulk transport is gradually lowered, leaving R_{cs} as the major contribution to the R_{ct}. What is more, from the pattern of contours in Fig. 6, one can see that any targeted effective cathode resistance R_{ct} may be well realized by tailoring materials parameters σ_s and σ_c. However, such a tailoring operation is restricted for each targeted R_{ct} by a lower limit of σ_s, below which no suitable cathode ionic conductivities can be found. This result significantly suggests that the oxygen surface reaction rate σ_s may set up a bottleneck to the cathodic kinetics of a porous MIEC cathode.

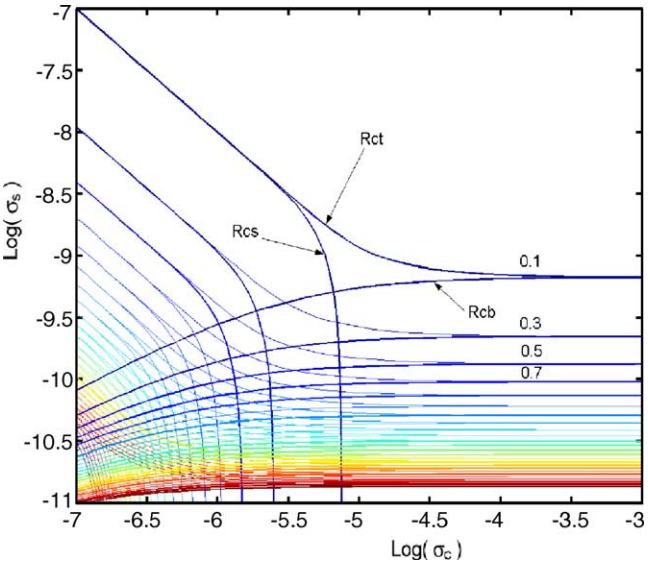

Fig. 6. Equal-resistance contours with $\log(\sigma_s)$ vs. $\log(\sigma_c)$.

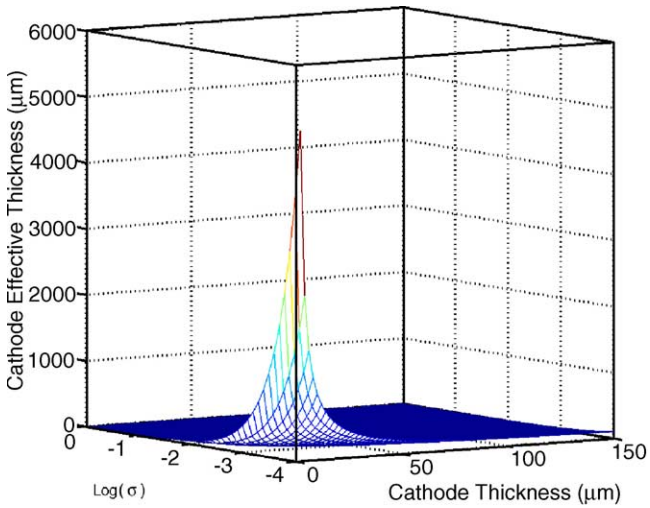

Fig. 7. Effective cathode thickness vs. real cathode thickness and $\log(\sigma_s/\sigma_c)$.

As regards the effective cathode thickness, it can be seen from Fig. 7 that the cathode has an effective thickness that first slightly increases from a value much lower than its real thickness as the real cathode thickness or $\log(\sigma_s/\sigma_c)$ decreases. But it undergoes an increasingly fast multiplication to a large value up to an infinite when the real thickness is greatly reduced down to zero. The details in the change of cathode effective thickness can be identified from a series of equal-effective thickness contours, as shown in Fig. 8, which helps reach a quantitative understanding of how the effective cathode thickness changes with the real cathode thickness and $\log(\sigma_s/\sigma_c)$.

3.3. I–V performance from 2D models

One 2D simulation of potential distribution has been firstly carried out to fulfill a direct comparison with the results from

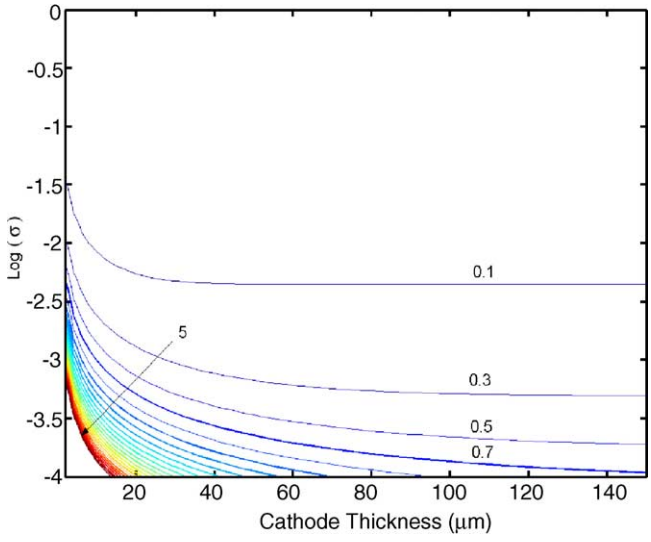

Fig. 8. Contours of effective cathode thickness with real cathode thickness vs. $\log(\sigma_s/\sigma_c)$.

the 1D model. The model was a solid belt with a length of 120 μm but different widths ξ. It is assumed that the oxygen surface incorporation is confined along the belt's two lateral lines and its reaction kinetic rate σ_s is evaluated with 2.5×10^{-9} times ξ to keep the same opportunity for ionic current injection per unit belt width, along with an output current density at cathode-electrolyte interface $q = 1$ (A cm^{-2}). It is very intriguing to find that, in the belt models with different widths ranging from 0.5 to 5 μm, the obtained potential distributions may be considered the same as in the case of 1D model when a difference of no larger than 0.0001 V is tolerated. This calculation result discloses an easily understandable but significant fact that the potential distribution is not immediately sensitive to the second dimension for a long belt model and it gives an electrochemical behavior extremely close to that of 1D cathode bar. Moreover, it may be derived that for real 3D cathodes a structural heterogeneity with characteristic length-scale much shorter than 5 μm might not remarkably impact the overall performance of cathodes. Further support for this point can be seen in the following analyses.

As shown in Fig. 9, the solid and porous belt models were given the same overall sizes 100 μm × 4 μm. In the porous belt, totally 50 spherical pores with an equal diameter of 1.7480 μm were uniformly distributed to realize a porosity of 30%. The boundary conditions for the former were set: $\sigma_s = 5 \times 10^{-9}$ for each lateral line, $\sigma_c = 1 \times 10^{-6}$ (S μm^{-1}), q = 0 and 1 (A cm^{-2}) at cathode depth $x = 0$ and 100 μm, respectively. For the latter, the same considerations were made to the boundary conditions except that the local current density at the right cathode end was increased to 4/2.250 = 1.7762 (A cm^{-2}) so as to achieve an apparent current density $q = 1$ (A cm^{-2}) for the presence of a half spherical void there. With such boundary conditions, the numerical calculations by a finite element algorithm demonstrated that the solid belt model gave an effective areal resistance of 0.1997 (Ω cm^{-2}) and the porous one had a resistance of 0.2277 (Ω cm^{-2}), 14.02% higher than the former. These results are quite meaningful if one has a careful comparison of their boundary conditions. For the porous belt, its oxygen incorporation interface boundary is actually 37.29% longer than that of the solid one, from 200 to 274.58. This greatly benefits the decrease of effective cathode areal resistance. But, on the other hand, the porous model has a lower effective ionic conductivity than the solid one. According to the mean field theory [42,43], it has been estimated that a porosity of 30% accounts for a 39.13% decrease in the effective conductivity. It can be seen, therefore, that a great decrease in the effective ionic conductivity of a porous MIEC cathode would considerably deteriorate the electrochemical performance of cathodes.

To further extend the above analyses, another simulation has been made with the assumption that the porous belt model has the equivalent oxygen surface incorporation rate constant and ionic conductivity to that of the solid one. So, the oxygen surface reaction rate σ_s for the porous belt model was set proportionally down to 3.6419×10^{-9} ($5 \times 10^{-9} \times 200/274.5800$) and its bulk ionic conductivity σ_c up to 1.6428×10^{-6} ($1 \times 10^{-6}/0.6087$) in terms of the mean field theory. With these modifications, the numerical calculation gave the porous belt model an almost the same potential distribution profile as that of the solid one, as illustrated in Fig. 10, telling an areal effective resistance of 0.2087 (Ω cm^{-2}) for the porous model. This value is certainly very close to that of the solid belt regardless of a small difference (4.50%), presumably attributed to the presence of pores characterized by their size distribution and spatial positions in the belt. Such a calculation result seems to disclose the same fact as in the previous paragraph that the presence of structural heterogeneity of length scale much shorter than 5 μm would not bring about

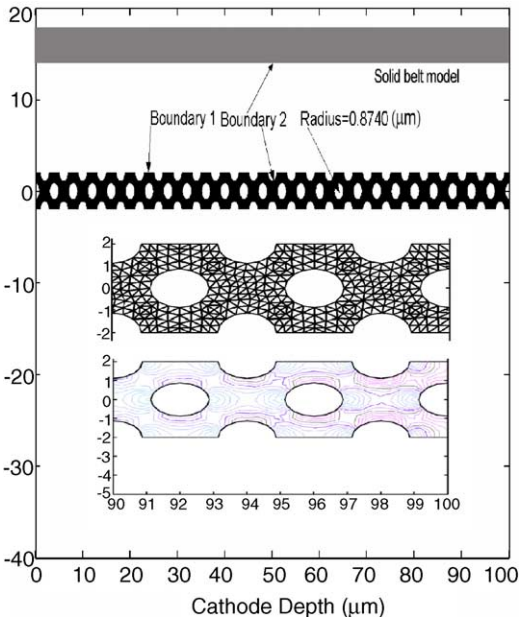

Fig. 9. Solid and porous 2D models, insets: A triangular network for finite element simulation (middle) and the contours of current density in it.

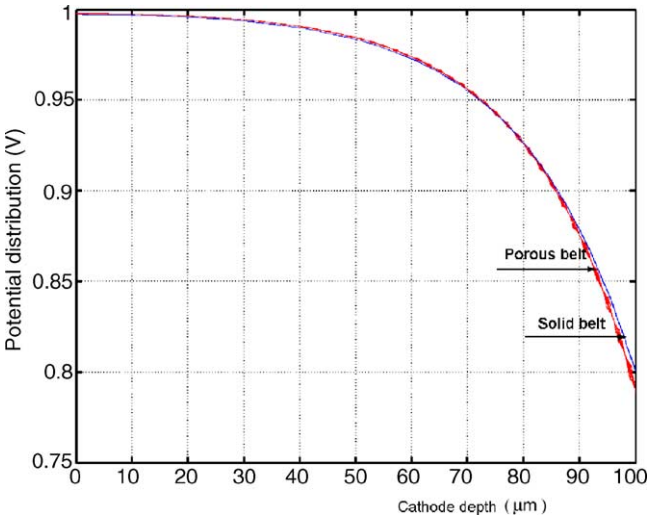

Fig. 10. Comparison of potential distributions from the porous model and the solid one.

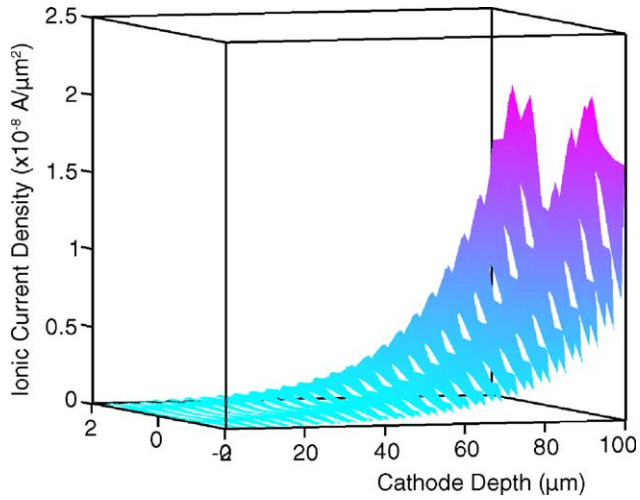

Fig. 11. Current density distribution over the 2D porous MIEC cathode.

a striking influence on the overpotential or effective areal resistance of cathodes if only they possess macro-statistically the same materials properties and geometric features. On the other hand, however, the structural heterogeneity may greatly impact the ionic current density distribution in cathodes, as shown in Fig. 11. It changes from a smooth distribution profile in the solid belt, see the solid continuous curve in Fig. 12, to a porous band with growing and fluctuating amplitude as the porous cathode depth increases. Such a pattern of current density distribution may be ascribed to the fact that the more close to the cathode-electrolyte interface is the pore-cathode interface situated, the more oxygen ionic flux takes its origin from it, the more inhomogeneous and strong local electric field gradient is caused, and thus the higher fluctuation in current density is induced, strongly depending on the local microstructural details. Obviously, this sensitive response of current density distribution to the microstructural details should be fully noted when a kinetic process controlled by local current density is concerned.

3.4. Impacts from interfacial graded structures

In above discussions, the cathode material is assumed to be uniform on certain relatively small scale either in its chemistry, grains microstructure or in its pore structure. But some relatively large scale structural inhomogeneity is likely to occur in cathodes, for instance, notable pore structural deviation from the average in the area adjacent to electrolytes. It can be expected that a more open porous structure in this bordering area is surely detrimental to the cathode's electrochemical properties because both oxygen surface incorporation and bulk transport in the area will be deteriorated, leading to an increase in the total areal resistance. However, what happens when a less porous (denser) structure is present in the neighboring area to the electrolyte? In order to make clear this issue, an interfacial structure model was introduced with the following gradient profile function:

$$\chi = \frac{h}{1 + [(x - t_c)/w]^2} \tag{12}$$

where h and w are the profile characteristic height and width adopted to describe the extent to which the structure-related property is modified in the interfacial area. The function's typical graphs with respect to different characteristic widths are shown in Fig. 13.

To take into account the effects from interfacial structure, it has been simply assumed that the oxygen surface transfer rate across the whole thickness was modulated by a decaying factor $(1 - \chi)$ with $h = 1$ and the ionic conductivity of cathode was controlled by an enhancing factor of $(1 + \chi)$ with $h = 0.6854$, in view of the fact that an additional ionic conductivity of $0.6854\sigma_c$ can be realized when a porosity of 30% is reduced to zero. With such assumptions, the effective areal resistances have been numerically calculated on a

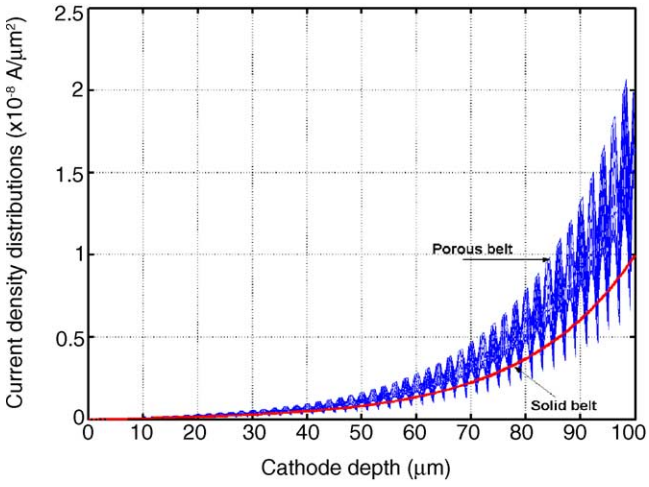

Fig. 12. Front view of current density distributions over the 2D porous belt model and the solid one.

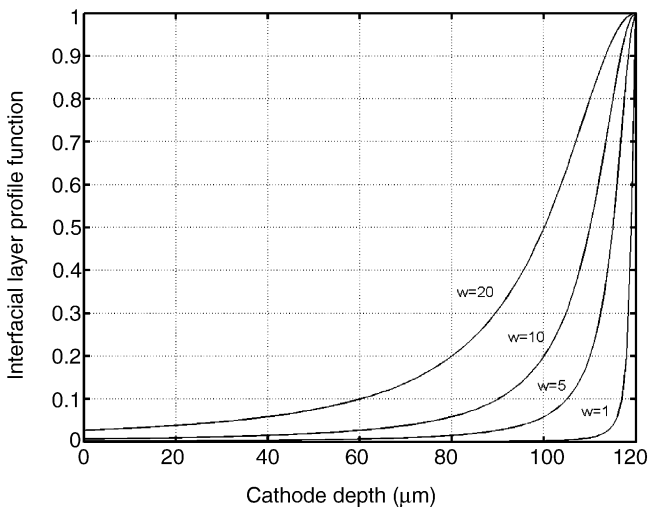

Fig. 13. Interfacial layer profiles with different characteristic widths.

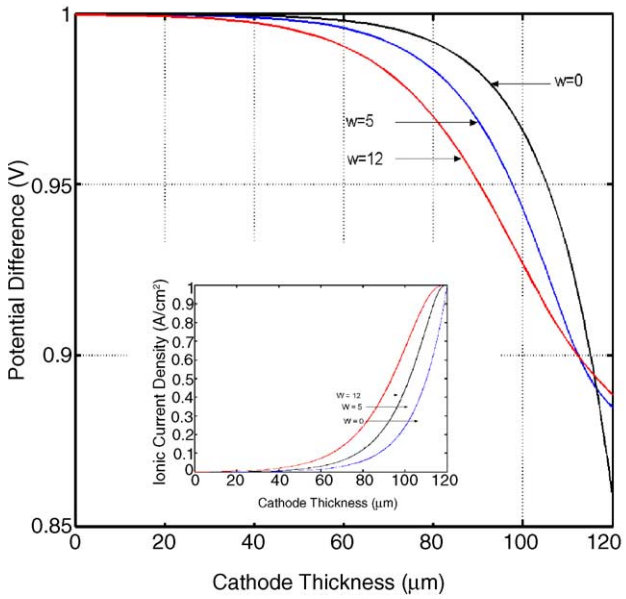

Fig. 14. Potential and current density (inset) distributions vs. different interfacial characteristic widths.

120 μm × 4 μm 2D model with regards to different characteristic widths of interfacial area. The calculation results of potential distribution and the change in effective cathode areal resistance are illustrated in Figs. 14 and 15. It can be observed that the graph A in Fig. 15 shows a simple increase in the effective cathode areal resistance as the dense interfacial area is broadened. This result suggests that such a densification of interfacial structure is by no means beneficial to the overall performance of cathode despite an additional ionic conductivity available in the interfacial area presumably for the reason that a sacrifice of the inner surface area where oxygen is incorporated into the cathode is much greater than the enhancement of ionic conductivity in that area. Therefore, it can be inferred that a gradually densified interfacial structure bordering the electrolyte is not helpful to the performance enhancement of a porous MIEC cathode composed of a single solid phase material.

However, what happens when a second phase with higher ionic conductivity than that of the matrix phase is introduced into that interfacial area of the cathode and would a remarkable decrease in the effective areal resistance of cathode be provoked? To verify this idea, some calculations similar to the above but with $h = 6.854$ (10 times as high as that of the matrix phase) have been performed and the results are shown as graph B in Fig. 15. It can be seen that the effective cathode resistance is indeed decreased in such cases. In particular, it decreases quite fast as the characteristic width w increases initially, then it slows down over a range before switches up to a growth. The maximum cut-down of the resistance is estimated as 0.050 ($\Omega\,cm^{-2}$) at the interfacial characteristic width $w = 12$ μm. It is about 10% down from a total resistance of 0.1414 ($\Omega\,cm^{-2}$) for the cathode without second phase, as given by either 1D or 2D model.

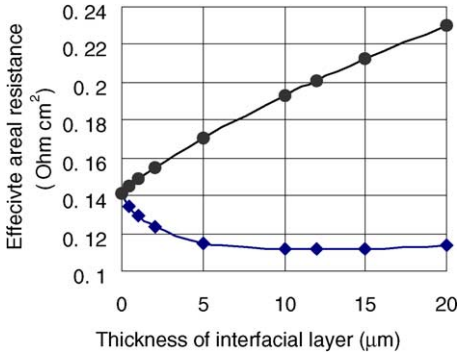

Fig. 15. Effective areal resistance vs. characteristic thickness of interfacial layer (μm): A (top); B (bottom).

4. Concluding remarks

On the basis of the above simulation results and extended discussions, the electrochemical behavior of porous mixed conducting cathodes can be outlined as follows:

1. In porous mixed conducting cathodes, the oxygen surface incorporation and bulk transport process are always convoluted together and this makes it difficult to fully understand how each cathodic process impacts the overall electrochemical performance of the cathode. By using model simulations, a clear and comprehensive understanding of these processes and their contributions to the global cathode performance has been achieved.
2. The structural heterogeneity scaled down to a few micros in MIEC cathodes is found not to remarkably affect their overall performance when they macro-statistically possess the same materials properties.
3. In comparison with 2D models, 1D model simulation may also provide a pretty good profile of potential distribution and thereby a measure of overpotentials due to oxygen surface incorporation and ionic transport in a porous MIEC cathode. In contrast, the details of current density distribution in porous MIEC cathodes have been observed via 2D models instead of 1D ones, strongly depending on the particular structural features of pores.
4. Among the materials parameters, the oxygen surface incorporation kinetic rate constant σ_s is of particular importance for the performance of porous MIEC cathodes. As a bottleneck, it acts to control the minimum effective cathode areal resistance even when the cathode has a very great ionic conductivity.
5. A structure-graded interfacial area bordering the electrolyte phase may conspicuously modify the cathode performance negatively or positively. The densified interfacial structure composed only of matrix material brings about a simple increase in effective cathode areal resistance. But an addition of second phase with higher ionic conductivity than that of the matrix to form a graded interfacial structure may improve the cathode performance.

Acknowledgements

The authors would like to gratefully acknowledge the financial support (Grant BK2002018) from The Science foundation of Jiangsu, PR China (2002).

References

[1] K.R. Kendall, C. Navas, et al., Solid State Ionics 82 (1995) 215–223.
[2] B.C.H. Steele, Solid State Ionics 134 (2000) 3.
[3] H. Yokokawa, N. Sakai, T. Horita, K. Yamaji, Fuel Cell 1 (2001) 117.
[4] S.J. Skinner, Int. J. Inorg. Mater. 3 (2) (2001) 113–121.
[5] F. Kundracik, M. Hartmanova, et al., Mater. Sci. Eng. B 84 (2001) 167–175.
[6] C.S. Song, Catal. Today 77 (2002) 17–49.
[7] K. Kobayashi, I. Takahashi, et al., Solid State Ionics 152 (2002) 591–596.
[8] R.R. Peng, C.R. Xia, X.Q. Liu, et al., Solid State Ionics 152 (2002) 561–565.
[9] E. Ivers-Tiffee, A. Weber, et al., J. Eur. Ceram. Soc. 21 (2001) 1805.
[10] O. Yamamoto, Electrochim. Acta 45 (2000).
[11] A. Endo, H. Fukunaga, et al., Solid State Ionics 135 (2000) 353.
[12] J. Mizusaki, Y. Yonemura, et al., Solid State Ionics 132 (2000) 167.
[13] B. Gharbage, T. Bagnier, A. Hammou, J Electrochem. Soc. 141 (1994) 2118.
[14] S.P. Jiang, J.G. Love, et al., Solid State Ionics 121 (1999) 1.
[15] Y. Matsuzaki, I. Yasuda, Solid State Ionics 126 (1999) 307.
[16] S.P. Jiang, Solid State Ionics 146 (2002) 1.
[17] Y. Teraoka, T. Nobunaga, et al., Solid State Ionics 48 (1991) 207.
[18] M. Mogensen, S. Skaarup, Solid State Ionics 86–88 (1996) 1151.
[19] B.C.H. Steele, Solid State Ionics 86–88 (1996) 1223.
[20] H.Y. Tu, Y. Takeda, et al., Solid State Ionics 100 (1997) 238.
[21] S.B. Adler, Solid State Ionics 111 (1998) 125.
[22] T. Kawada, K. Masuda, et al., Solid State Ionics 121 (1999) 271.
[23] R.H.E. van Doorn, A.J. Burggraaf, Solid State Ionics 128 (2000) 65.
[24] T. Horita, K. Yamaji, N. SaItai, et al., Solid State Ionics 138 (2000) 143.
[25] B. Zhu, X.R. Liu, M. Sun, et al., Solid State Sciences 5 (2003) 1127.
[26] R.L. Wither, M. James, D.J. Goossens, J. Solid State Chem. 174 (2003) 198.
[27] S.P. Scott, D. Mantzavinos1, A. Hartley, et al., Solid State Ionics 152 (2002) 777.
[28] G.W. Coffey, J. Hardy, L.R. Pedersen, et al., Solid State Ionics 158 (2003) 1.
[29] H.Y. Tu, Y. Takeda, N. Imanishi, O. Yamamoto, Solid State Ionics 117 (1999) 277.
[30] L. Qiu, T. Ichikawa, A. Hirano, N. Imanishi, Y. Takeda, Solid State Ionics 158 (2003) 55.
[31] F. Zheng, R.K. Bordia, L.R. Pederson, Mater. Res. Bull. 39 (2004) 141.
[32] H.C. Yu, K.Z. Fung, Mater. Res. Bull. 38 (2003) 231.
[33] Y. Yamamuraa, C. Iharaa, S. Kawasakia, et al., Solid State Ionics 160 (2003) 93.
[34] J. Fleig, J. Power Sources 105 (2002) 228.
[35] V. Brichzin, J. Fleig, et al., Solid State Ionics 152 (2002) 499.
[36] S.B. Adler, J.A. Lane, et al., J. Electrochem. Soc. 143 (1996) 3554.
[37] S.B. Adler, Solid State Ionics 111 (1998) 125.
[38] A.M. Svensson, S. Sunde, et al., Solid State Ionics 86 (1996) 1211.
[39] A. Endo, H. Fukunaga, C. Wen, et al., Solid State Ionics 135 (2000) 353.
[40] D. Herbsrtritt, A. Weber, E. Ivers-Tiffee, J. Eur. Ceram. Soc. 21 (2001) 1813.
[41] H. Fukunaga, M. Ihara, et al., Solid State Ionics 86 (1996) 1179.
[42] N.H. Tallen, Electrical conductivity in ceramics and glass, Part B, Marcel Dekker, 1974, p. 628.
[43] D.S. Mclachlan, et al., J. Am. Ceram. Soc. 73 (1990) 2187.